Journal of Molecular Catalysis A: Chemical 332 (2010) 84–92

Contents lists available at ScienceDirect

Journal of Molecular Catalysis A: Chemical

journal homepage: www.elsevier.com/locate/molcata

TiO_2/V–TiO_2 composite photocatalysts with an n–n heterojunction semiconductor structure

Song Liu*, Jiantao Wu, Xingping Liu, Rongying Jiang

Department of Applied Chemistry, South China University of Technology, Guangzhou 510640, PR China

ARTICLE INFO

Article history:
Received 12 June 2010
Received in revised form 27 August 2010
Accepted 1 September 2010
Available online 15 September 2010

Keywords:
Titania
n–n heterojunction
Photocatalysis
Composite
Vanadium

ABSTRACT

Highly active TiO_2/V–TiO_2 composite photocatalysts with an n–n heterojunction semiconductor structure have been prepared by mixing TiO_2 sol with sol–gel derived V–TiO_2 powders that have adsorbed ammonium oleate in advance, followed by drying and calcination. These composite photocatalysts were characterized by XRD, TEM, BET, XPS, UV–vis and PL spectroscopy. The photodegradation of methyl orange in aqueous solution under UV–vis light irradiation has been investigated over TiO_2-based photocatalysts consisting of different TiO_2/V–TiO_2 ratios and different vanadium contents. TiO_2/V–TiO_2 composite photocatalysts were generally shown to have a much higher photocatalytic destruction rate than that of undoped TiO_2, which is ascribed mainly to the electrostatic-field-driven electron–hole separation in TiO_2/V–TiO_2 composite photocatalysts. The best TiO_2/V–TiO_2 composite with the mass ratio of TiO_2:0.5 at.%V–TiO_2 equal to 12:1 demonstrates 5.9 times the photocatalytic activity of that of undoped TiO_2 with comparable crystallite size and specific surface area. The effect of photocatalysts composition on the photoactivity was discussed.

© 2010 Elsevier B.V. All rights reserved.

1. Introduction

Titania is well known as a cheap, stable, nontoxic, and efficient photocatalyst without secondary pollution. However, the efficiency of the photocatalytic degradation reaction is limited by the high recombination rate of photoinduced electrons and holes. Many attempts have been made to suppress the recombination by doping titania with metal ions [1,2]. Among the transition metal ions, vanadium ion is attractive because vanadium doping can increase carrier lifetime [3] and apparently also extend the absorption range of TiO_2 [1,2,4–33]. Vanadium-doped TiO_2 samples have been the object of many papers, including preparation and characterization, spectroscopic features, dynamics of charge-transfer trapping and photocatalytic behavior [1–33].

To suppress the photogenerated electron–hole recombination, another approach is to couple titania with other semiconductor materials or couple different titania polymorphs materials (or to prepare mixed-phase titania particles), such as TiO_2/GaP [34], TiO_2/CdS [35–45], TiO_2/Bi_2S_3 [45], TiO_2/SnS_x [46], TiO_2/MoS_2 [47], TiO_2/WS_2 [47], TiO_2/PbS [48], TiO_2/CdSe [49], TiO_2/ZnO [44,50–53], TiO_2/Fe_2O_3 [35], TiO_2/NiO [54], TiO_2/Cu_2O [55–57], TiO_2/Bi_2O_3 [56], TiO_2/SnO_2 [58–64], TiO_2/WO_3 [65–66], TiO_2/In_2O_3 [67], TiO_2/$ZnMn_2O_4$ [56], TiO_2/$FeTiO_3$ [68–70], TiO_2/$LaVO_4$ [71], TiO_2/$InVO_4$ [72], TiO_2/$CuAlO_2$ [73], TiO_2/BDD [74,75], TiO_2/$Sr(Zr_{1-x}Y_x)O_{3-\delta}$ [76], and TiO_2/Si [77]. Recently, Kang et al. [78] prepared the TiO_2/N–TiO_2 composites by grinding in ethanol solvent. Wang and co-workers [79,80] have SnO_2/α-Fe_2O_3 and nano-composite with Fe-doped anatase TiO_2 nanoparticles coupling with TiO_2(B) nanobelts. These composites tend to show higher photoactivity in comparison to single-phase titania materials, due to the formation of solid–solid interfaces that facilitate charge transfer and spatial separation, reduced electron–hole recombination, and interface defect sites that act as catalytic "hot spots".

In previous paper [81], we prepared a kind of TiO_2/V–TiO_2 composite powders by a so-called uneven doping method, i.e. by mixing TiO_2 sol with sol–gel derived V–TiO_2 powders, followed by drying and calcination (coupling pure TiO_2 nanoparticles with V–TiO_2 nanoparticles). The as-prepared samples (composites) were shown to have a much higher photocatalytic destruction rate than that of sol–gel-derived V–TiO_2 photocatalysts and undoped TiO_2, due to the formation of junction between undoped TiO_2 with V–TiO_2 nanoparticles.

In the present paper, we prepared the highly active TiO_2/V–TiO_2 composite photocatalysts by a modified method using ammonium oleate in order to improve the structure of n–n heterojunction, i.e. by mixing TiO_2 sol with sol–gel derived V–TiO_2 powders that have adsorbed ammonium oleate in advance, followed by drying and calcination. It was found that the photocatalytic activity of the catalysts prepared by the new method was enhanced since the addition of ammonium oleate could increase the interface region of catalysts. The energy-band diagrams of TiO_2/V–TiO_2 composite photocatalysts were presented and a hypothetical configuration of

* Corresponding author. Tel.: +86 020 87114875; fax: +86 020 87112906.
E-mail address: chsliu@scut.edu.cn (S. Liu).

1381-1169/$ – see front matter © 2010 Elsevier B.V. All rights reserved.
doi:10.1016/j.molcata.2010.09.003

composite photocatalysts was proposed. The role of heterojunction and the effect of the molar ratio of titania of undoped TiO_2 to that of V–TiO_2 and vanadium dopant concentration on the photoactivity were discussed.

2. Experimental

2.1. Preparation

All the reagents were of analytical grade and used without further purification. Tetrabutyl titanate was chased from Shanghai Chemical Reagent Co., oleic acid was chased from Sinopharm Chemical Reagent Co., and the other reagents were chased from Guangzhou Chemical Reagent Co. All solutions were prepared with bidistilled deionized water.

Pure titania catalyst using tetrabutyl titanate as a titanium precursor was synthesized using the sol–gel method at room temperature. 40 mL of absolute ethyl alcohol, 10 mL of glacial acetic acid and 5 mL of double-distilled water were mixed as solution a, then it was added drop-wise under vigorous stirring into the solution *b* that contains 17 mL of tetrabutyl titanate and 40 mL of absolute ethyl alcohol. The resulting transparent colloidal dispersion (marked as TiO_2-sol) was stirred for 0.5 h and aged for 2 days till the formation of xerogel, then grounded into powder. The powder was calcined at 500 °C for 3 h, and then grounded in agate mortar to obtain fine titania powders finally.

Several TiO_2 powders doped by V evenly (abbreviated hereafter as VTE) were generated using the sol–gel method at room temperature by taking precursor NH_4VO_3. 40 mL of absolute ethyl alcohol, 10 mL of glacial acetic acid and 5 mL of double-distilled water and the required amounts of NH_4VO_3 were mixed as solution *c*, and then it was added drop-wise under vigorous stirring into the solution *b*. The following procedures were carried according to the pure titania. The V–TiO_2 catalysts had a nominal atomic ratio (V/Ti) of *z*%, so they are named as *z*%V–TiO_2 in this study.

A series of the TiO_2/V–TiO_2 composite powders (abbreviated hereafter as VTU) were generated at room temperature with the following procedure: the required amounts of 0.5%V–TiO_2 powders (VTE) were put into transparent TiO_2-sol above-mentioned under stirring and the resulting suspension was stirred continuously for 3 days (during the 3 days, the solvent volatilized slowly). Then, the mixture was dried at 100 °C for 4 h, and fired at 500 °C for 3 h. The as-prepared photocatalysts are named hereafter *y*TiO_2/0.5%V–TiO_2, *y* is the nominal molar ratio of titania of TiO_2-sol to that of 0.5%V–TiO_2 (i.e. the nominal molar ratio of titania of undoped TiO_2 to VTE).

Three series of the TiO_2/V–TiO_2 composite powders (abbreviated hereafter as VTMU) were prepared by the modified method described as follows. Firstly, 3 g *z*%V–TiO_2 (*z* are 0.04, 0.5 and 2.0, respectively) powders were sonicated in 30 mL of 0.17 M ammonium oleate aqueous solution (generated by mixing equal moles of ammonia with oleic acid) for 1 h and then stirred for 2 h. Secondly, the solids were separated by centrifugation and washed 3 times with ethanol. The purified powders were dried at 60 °C for 4 h and cooled at room temperature (the as-prepared powders are named hereafter *z*%V–TiO_2-O). Thirdly, the required amount of *z*%V–TiO_2-O powders was put into TiO_2-sol under stirring and the resulting suspension was stirred continuously for 3 days. Finally, the mixture was dried at 100 °C for 4 h, and fired at 500 °C for 3 h. The as-prepared photocatalysts are named hereafter as *y*TiO_2/*z*%V–TiO_2/M.

2.2. Characterization

Powder XRD patterns for samples were recorded using a Bruker D8 Advance diffractometer with Ni-filtered Cu-Kα radiation (λ = 0.154056 nm). The average crystal sizes were calculated from the X-ray diffractograms by the Scherrer formula. A transmission electron microscope (TEM), JEM-2010, was applied to observe the morphology of catalysts and estimate the particle size. The surface area of catalysts was determined using a standard Brunauer–Emmett–Teller (BET) apparatus (Micromeritics TristarII3020). The pore size distribution of the catalysts was determined by the Barrett–Joyner–Halenda (BJH) method. Diffuse reflectance UV–vis spectra were recorded on a Hitachi UV-3010 spectrometer equipped with an integrating sphere of 60 mm in diameter using $BaSO_4$ as a standard. Photoluminescence spectra were collected on a Fluorescence spectrometer (Hitachi F-4500) with a powder holder accessory under room temperature. The catalysts of X-ray photoelectron spectroscopy data were obtained through a Kratos Axis Ultra (DLD) electron spectrometer from VG Scientific under 300-W AlKα radiation. The base pressure was about 3×10^{-9} mbar. The binding energies were referenced to the C 1s line at 284.6 eV from adventitious carbon.

2.3. Photoreactivity measurements

Photocatalytic decolorization of methyl orange in an aqueous medium was used as a probe reaction to access the photocatalytic activity of all the powders. A Pyrex cylindrical photoreactor with an effective volume of 250 mL was used to conduct photocatalytic degradation experiments, which was surrounded by a Pyrex circulating water jacket. An 8-W UV lamp (Toshiba, Inc.) with a main emission at 365 nm was located at the center of the cylindrical vessel and used for photoreaction. For each experiment, 200 mg of photocatalyst was added to 250 mL of 5 mg/L methyl orange solution stirred with a magnetic stirrer. The aerated suspension was first stirred in the dark for 60 min, which was sufficient to reach adsorption equilibrium of methyl orange. The concentration of aqueous methyl orange was determined with a Hitachi UV-3010 spectrometer by measuring the absorbance at 464 nm.

3. Results

3.1. Photocatalytic activity

Fig. 1 displays the decrease of methyl orange concentration as a function of UV light irradiation time over TiO_2-based photocatalysts. The photocatalytic activity of commercial Degussa P25 TiO_2 catalysts prepared by flame pyrolysis was also included for

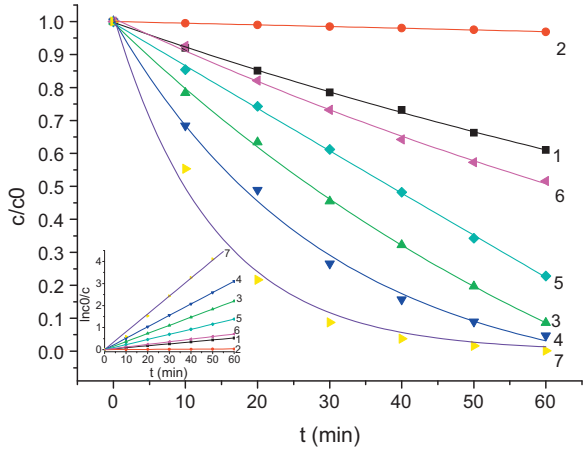

Fig. 1. Decrease of methyl orange concentration as a function of UV irradiation time over the different catalysts: (1) undoped TiO_2, (2) 0.5%V–TiO_2, (3) 12TiO_2/0.5%V–TiO_2, (4) 12TiO_2/0.5%V–TiO_2/M, (5) 12TiO_2/0.04%V–TiO_2/M, (6) 12TiO_2/2%V–TiO_2/M, and (7) P25.

Table 1
Samples preparation condition and results.

Sample	Apparent rate constant (min^{-1})	Specific surface area ($m^2\ g^{-1}$)	$N_{nn} \times 10^{-18}$
Undoped TiO_2	0.0081	50.7	
0.5%V–TiO_2	0.0005	57.4	
12TiO_2/0.5%V–TiO_2	0.0338	59.3	
12TiO_2/0.04%V–TiO_2/M	0.0211	66.3	
12TiO_2/2%V–TiO_2/M	0.0109	64.6	
4TiO_2/0.5%V–TiO_2/M	0.0133		3.99
4.4TiO_2/0.5%V–TiO_2/M	0.0148		4.08
5TiO_2/0.5%V–TiO_2/M	0.0194		4.16
5.7TiO_2/0.5%V–TiO_2/M	0.0211		4.25
6.7TiO_2/0.5%V–TiO_2/M	0.0284		4.34
8TiO_2/0.5%V–TiO_2/M	0.0397		4.44
10TiO_2/0.5%V–TiO_2/M	0.0413		4.54
11TiO_2/0.5%V–TiO_2/M	0.0421		4.57
12TiO_2/0.5%V–TiO_2/M	0.0478	66.3	4.6
13.3TiO_2/0.5%V–TiO_2/M	0.0365		4.18
20TiO_2/0.5%V–TiO_2/M	0.0219		2.85
40TiO_2/0.5%V–TiO_2/M	0.0211		1.46
Mechanical mixture[a]	0.0081		
P25	0.081		

[a] The molar ratio of undoped TiO_2 to 0.5%V–TiO_2 is 12.

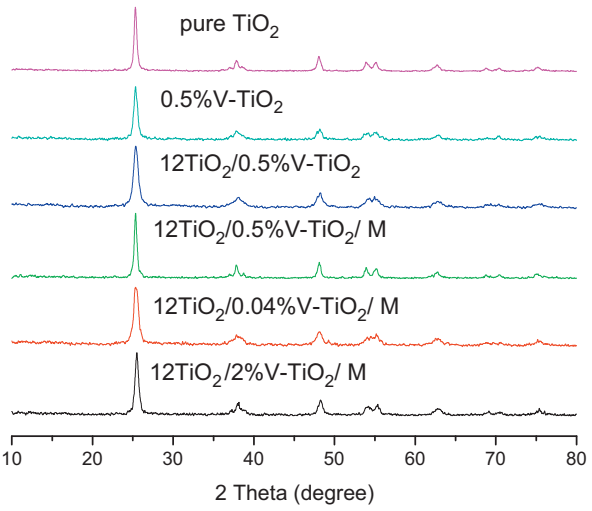

Fig. 3. XRD patterns of catalysts.

comparison. The photocatalytic decolorization of methyl orange is an apparent first-order reaction verified by the linear transforms $\ln c_0/c = f(t)$ illustrated in the insert in Fig. 1. To enable quantitative comparison, the apparent rate constants (displayed in Table 1 and Fig. 2) were calculated to represent the photoactivities.

From Table 1 and Fig. 2, it was observed that many samples of TiO_2/V–TiO_2 composite photocatalysts exhibited much higher photocatalytic activity compared with VTE and undoped TiO_2 powders. It was obvious that 12TiO_2/0.5%V–TiO_2/M had the best photocatalytic activity whose apparent rate constant was about 5.9 times as large as that of undoped TiO_2, and about 1.4 times as large as that of 12TiO_2/0.5%V–TiO_2 with the same chemical composition as 12TiO_2/0.5%V–TiO_2/M.

According to the experimental results of photocatalytic activity, six photocatalysts were selected for a detailed characterization.

3.2. Characterization

XRD patterns of the TiO_2-based nanoparticles are shown in Fig. 3. The patterns can be indexed to the anatase phase only, and no separate VO_x phases were observed for any of the vanadium-containing samples because of their low concentration in the catalyst. Based on data given by Rodella et al. [82], we believe that all vanadium is dispersed throughout TiO_2 as vanadyl groups (V^{4+}) and/or polymeric vanadates (V^{5+}) rather than crystalline V_2O_5. The grain sizes estimated from the peak broadening of undoped titania, 0.5%V–TiO_2, 12TiO_2/0.5%V–TiO_2, 12TiO_2/0.5%V–TiO_2/M, 12TiO_2/0.04%V–TiO_2/M and 12TiO_2/2%V–TiO_2/M were 22.5 nm, 20.4 nm, 24.2 nm and 24.5 nm, 24.0 nm and 24.6 nm, respectively, indicating that the grain size of TiO_2/V–TiO_2 composites was slightly larger than that of undoped titania.

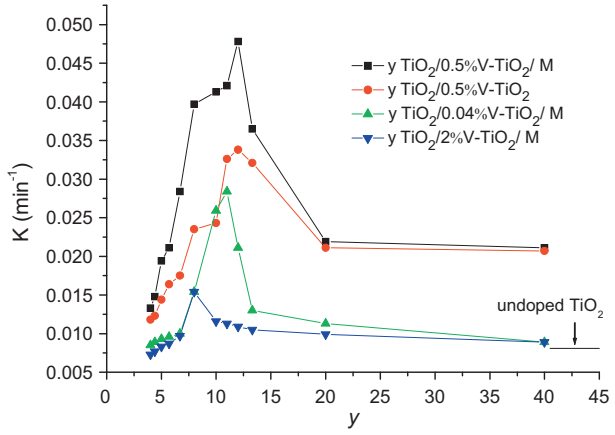

Fig. 2. The apparent rate constants of catalysts.

TEM images in Fig. 4 reveal that the prepared samples consisted of aggregates of primary particles of 10–35 nm in diameter, which is in general agreement with the XRD determination.

The N_2 adsorption–desorption isotherms of catalysts in Fig. 5 are characteristic type-IV curves according to the BDDT classification with hysteresis loops [83]. The BET surface areas of the photocatalysts are summarized in Table 1. The specific surface areas of the TiO_2/V–TiO_2 composites were larger by about 20–30% than that of undoped titania. The BJH pore size distributions calculated on the basis of the desorption branch of the isotherms are shown in Fig. 6. The diameter range of the most pores was from 3 to 12 nm and the average pore diameter was about 4.2–6.9 nm. The formation of mesoporous structure in the samples is attributed to the aggregation of TiO_2 crystallites [84].

XPS spectra of six samples were similar. Fig. 7 shows XPS spectra of the O 1s and Ti 2p of photocatalysts. The O 1s peak is found at 529.6 eV on the undoped TiO_2, and it shifts slightly to lower electron binding energy (BE) upon vanadium doping (for example, 529.4 eV for 0.5%V–TiO_2) [85–87]. The Ti $2p_{3/2}$ line is found at a BE of 458.4 eV on the undoped TiO_2, and it also shifts slightly to lower electron binding energy (BE) upon vanadium doping (for example, 458.2 eV for 0.5%V–TiO_2) [85–87]. The shift of the O 1s and Ti 2p XPS lines by an amount of ~0.3 eV to lower BE upon vanadium oxide deposition has already been demonstrated by Zhang and Henrich [85], and it has been attributed to a simple shift of the Fermi level into TiO_2 band gap. The O 1s peak can be fitted into two Gaussian peaks at about 529.6 and 531.4 eV, which arise from lattice oxygen (O^{2-}) of titania and surface hydroxyl groups on titania surface, respectively [88]. In addition, there was no signal of vanadium for vanadium-containing TiO_2, due to the low vanadium content.

Fig. 8 displays UV–vis DRS of TiO_2-based photocatalysts with insert showing plot of $(\alpha h\nu)^{1/2}$ versus energy ($h\nu$) [33,80]. As observed in Fig. 8, the absorption edge of undoped TiO_2, appeared at about 400 nm, corresponding to the band gap energy of about 3.1 eV. This value was close to the reported value of anatase (3.2 eV) [31]. Compared with undoped TiO_2, vanadium-containing titania samples exhibited a red shift of the absorption and showed

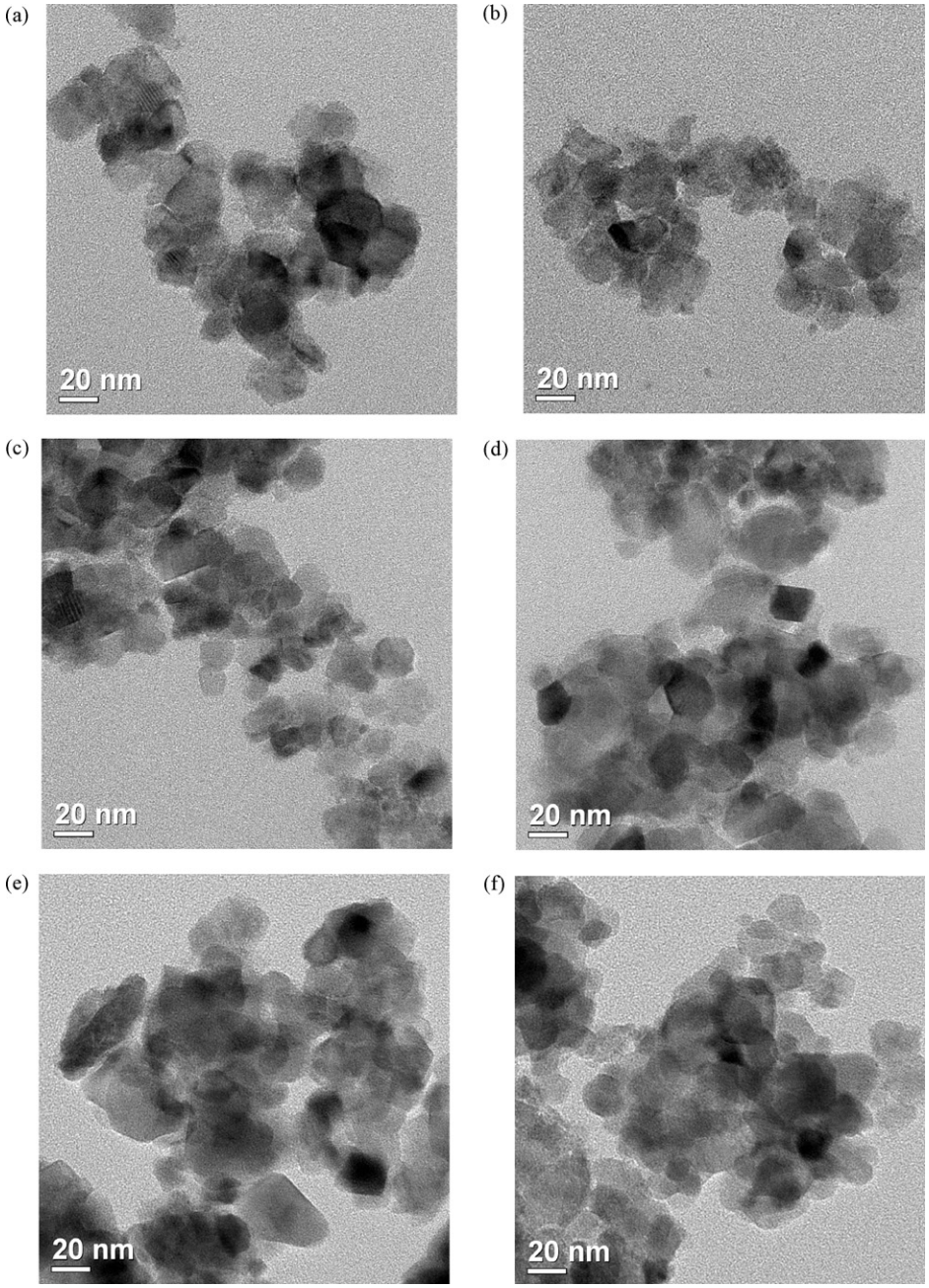

Fig. 4. TEM images of (a) undoped TiO_2, (b) 0.5%V–TiO_2, (c) 12TiO_2/0.5%V–TiO_2, (d) 12TiO_2/0.5%V–TiO_2/M, (e) 12TiO_2/0.04%V–TiO_2/M, and (f) 12TiO_2/2%V–TiO_2/M.

enhanced absorptions in the range from 400 to 600 nm with increasing vanadium content, accompanied with the changes on color from white to grey. The absorption edge of 0.5%V–TiO_2 appeared at about 460 nm, corresponding to the band gap energy of about 2.7 eV. For other vanadium-containing titania samples, the red shift is not obvious since the content of vanadium in these samples is low. The red shift and the tailing of the absorption band can be assigned to the charge-transfer transition from the d orbital of V^{4+} to the conduction band of TiO_2 [1,2,5], indicating the successful incorporation of vanadium ions into lattice [80,89]. The enhanced absorption in visible region is beneficial to the photocatalytic activity since more photons can be utilized.

Photoluminescence spectra of catalysts in Fig. 9 exhibit seven main emission peaks at about 399, 413, 421, 453, 469, 483 and 493 nm with excitation at 320 nm. High energy peaks can be assigned to edge luminescence of the TiO_2 particles, while lower energy peaks are introduced by the presence of the oxygen vacancies [90]. The great decrease in emission intensity of 0.5%V–TiO_2 compared with undoped TiO_2 may be due to the impurity levels introduced by dopant that enhanced non-radiative recombination of the excited electrons [2,91,92]. Similar quenching in the luminescence intensity has also been observed for V-, Fe-, W-, Zr-, Cu-, Ni-, Ga-, Cd-, Ag-, Al- and Pb-doped TiO_2 by Nagaveni et al. [2], Zhou et al. [93], Tang et al. [92] and Rahman et al. [91].

4. Discussion

The differences of structure and properties between TiO_2/V–TiO_2 composite photocatalysts (e.g. 12TiO_2/0.5%V–TiO_2/M) with pure titania were not large, but the photocatalytic activity of the former was much higher than that of the later, as indicated in the Section 3. The reason will be discussed as follows.

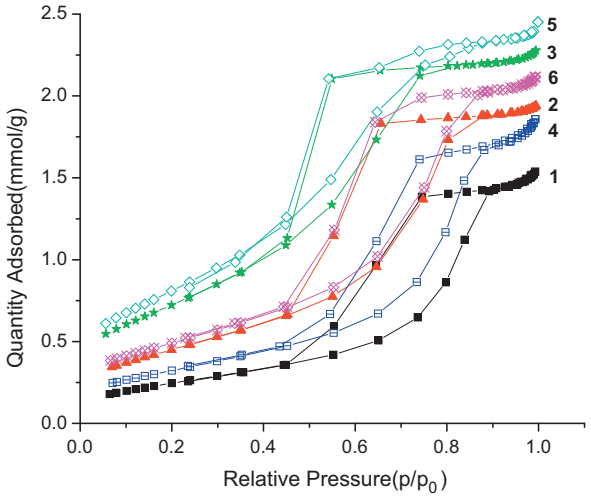

Fig. 5. Nitrogen adsorption–desorption isotherm for photocatalysts.

4.1. Role of n–n heterojunction

Liau and Chou [94] have prepared nano-TiO_2 electrodes by coating Fe-doped (or Cr-doped or Zn-doped) TiO_2 film on top of undoped TiO_2 film. It shows that these electrodes give a strong rectifying action, which is the characteristic of a heterojunction (TiO_2/Fe–TiO_2 or TiO_2/Cr–TiO_2 or TiO_2/Zn–TiO_2). Insofar that the conclusions of the cited investigation [94] can be transposed to the present case of TiO_2 and V–TiO_2, a heterojunction can be formed at the interfaces between TiO_2 with V–TiO_2 particles.

Serpone et al. [6], Herrmann et al. [95], Egdell et al. [96] and Zhao et al. [97] have prepared V-doped titania by controlled hydrolysis, impregnation, solid state reaction and sol–gel methods, respectively. The n-type semiconductor character for these V-doped titania was confirmed by photoconductivity, electrical conductivity, resistance and Hall constant measurements. The anatase is also n-type semiconductor [95].

Anderson et al. [98] have investigated the photocatalytic and electrophoretic mobility of V-doped titania thin-film and found that the flat band potential (which corresponds to the position of the Fermi level) of 0.5%V–TiO_2, 1%V–TiO_2, 2.5%V–TiO_2 and 5%V–TiO_2 was shifted positively by 80, 100, 180 and 300 mV with regards to that of undoped TiO_2 (anatase), respectively, which means that the Fermi energy of undoped TiO_2 is higher than that of V–TiO_2.

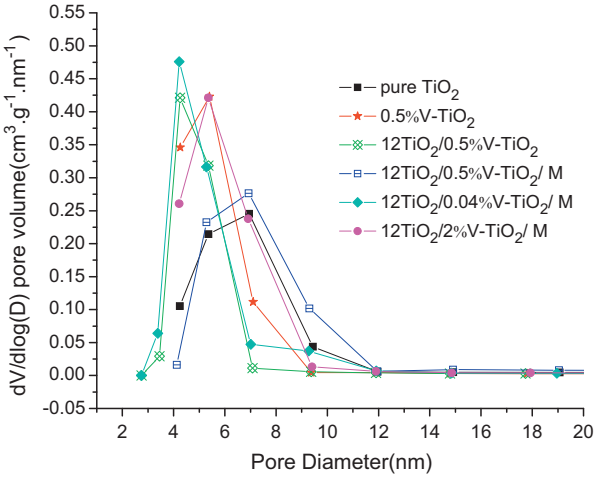

Fig. 6. Pore size distribution curve of photocatalysts.

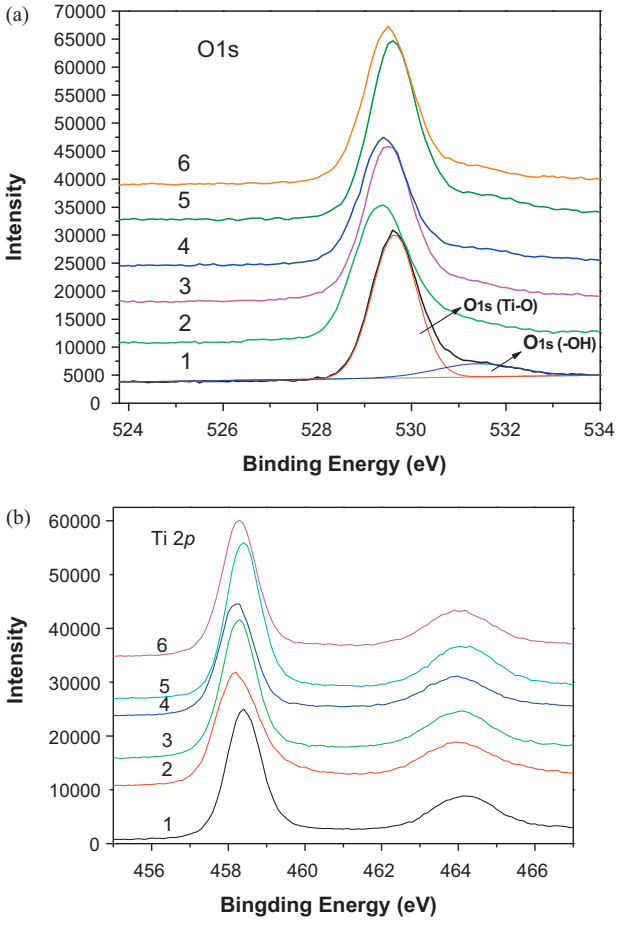

Fig. 7. XPS spectra of O 1s (a) and Ti 2p (b) of (1) undoped TiO_2, (2) 0.5%V–TiO_2, (3) 12TiO_2/0.5%V–TiO_2, (4) 12TiO_2/0.5%V–TiO_2/M, (5) 12TiO_2/0.04%V–TiO_2/M, and (6) 12TiO_2/2%V–TiO_2/M.

In the process of preparation of VTU and/or VTMU, after addition of *z*%V–TiO_2 or *z*%V–TiO_2-O into TiO_2-sol, a mixture of *z*%V–TiO_2 with amorphous undoped TiO_2 particles was obtained. In the subsequent process of calcination, amorphous undoped titania crystallized and combined with *z*%V–TiO_2 nanoparticles by sintering. Therefore, at the interfaces between *z*%V–TiO_2 with undoped anatase titania particles, an n–n heterojunction will be formed,

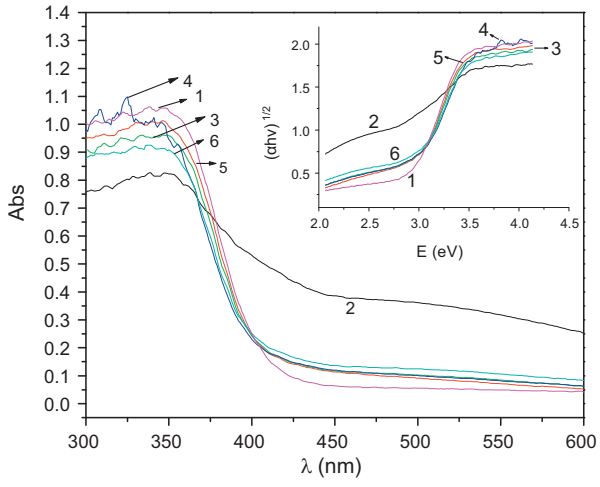

Fig. 8. UV–vis DRS of (1) undoped TiO_2, (2) 0.5%V–TiO_2, (3) 12TiO_2/0.5%V–TiO_2, (4) 12TiO_2/0.5%V–TiO_2/M, (5) 12TiO_2/0.04%V–TiO_2/M, and (6) 12TiO_2/2%V–TiO_2/M.

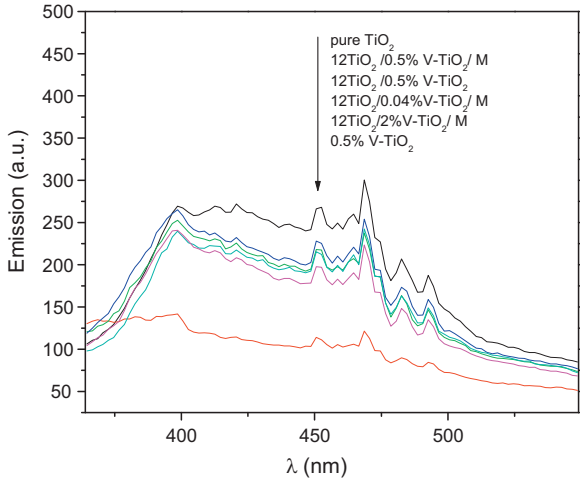

Fig. 9. Photoluminescence emission spectra of photocatalysts.

which was erroneously assigned to p–n junction in our previous paper [81] because we have confused the p–n conversion with p-type conductivity. Cheng and coworkers [99] have observed the phenomena of p–n conversion in V–TiO_2 electrode when monochromatic light of wavelength of 350 nm was used as incident light. They have measured the transient photocurrent at different electrode potentials and found that cathodic photocurrent (p-type photoresponse) appeared at negative potentials, and then converted to anodic photocurrent (n-type photoresponse) at positive potentials. We judged mistakenly that V–TiO_2 was p-type semiconductor by the phenomena of p–n conversion. In fact, the n-type semiconductor character of V–TiO_2 has been confirmed by photoconductivity, electrical conductivity, resistance and Hall constant measurements [6,95–97], as mentioned in forgoing paragraphs.

Because the Fermi level of anatase is higher than that of VTE [100], at an n–n heterojunction located at the juncture between anatase and VTE, electrons diffuse from anatase into VTE region, creating an accumulation of negative charges in the VTE region and a positive section in the anatase region in the vicinity of the junction. This sets up an internal electrostatic field directed from anatase to VTE region, creating an energy barrier for the electron transfer from anatase to VTE [101].

The energy-band diagrams of TiO_2/V–TiO_2 composite photocatalysts are shown in Fig. 10 [102–104]. In Fig. 10, the subscripts 1 and 2 refer to undoped titania and VTE; E_g is the band gap; x is electron affinity of the semiconductors; E_c and E_v are conduction and valence band edge, respectively; ΔE_c is the conduction band edge discontinuity (conduction-band offset), $\Delta E_c = x_2 - x_1$; ΔE_v is the valence band edge discontinuity, $\Delta E_v = (E_{g1} - E_{g2}) - (x_2 - x_1)$. In this paper, we assume that the Fermi level (E_F) of the semiconductors equals approximately the conduction band (E_c) [105].

Under irradiation, both anatase and VTE nanoparticles absorb the band-gap photons and then the electron–hole pairs are generated. Photo-generated holes and electrons separate under the influence of the internal electrostatic field in the n–n heterojunction region. Holes move to VTE side, and electrons to the anatase side. Thereby, the chance of electron–hole recombination is reduced. This leads to high photocatalytic activity of photooxidation of methyl orange. Moreover, large specific surface areas of TiO_2/V–TiO_2 composite photocatalysts are beneficial for the adsorption of methyl orange on the catalyst surface, which can enhance photocatalytic activity also.

A mechanical mixture of undoped TiO_2 and 0.5%V–TiO_2 was also tested for photodegradation (the molar ratio of undoped TiO_2 to 0.5%V–TiO_2 is 12). The photocatalytic activity of the mechanical

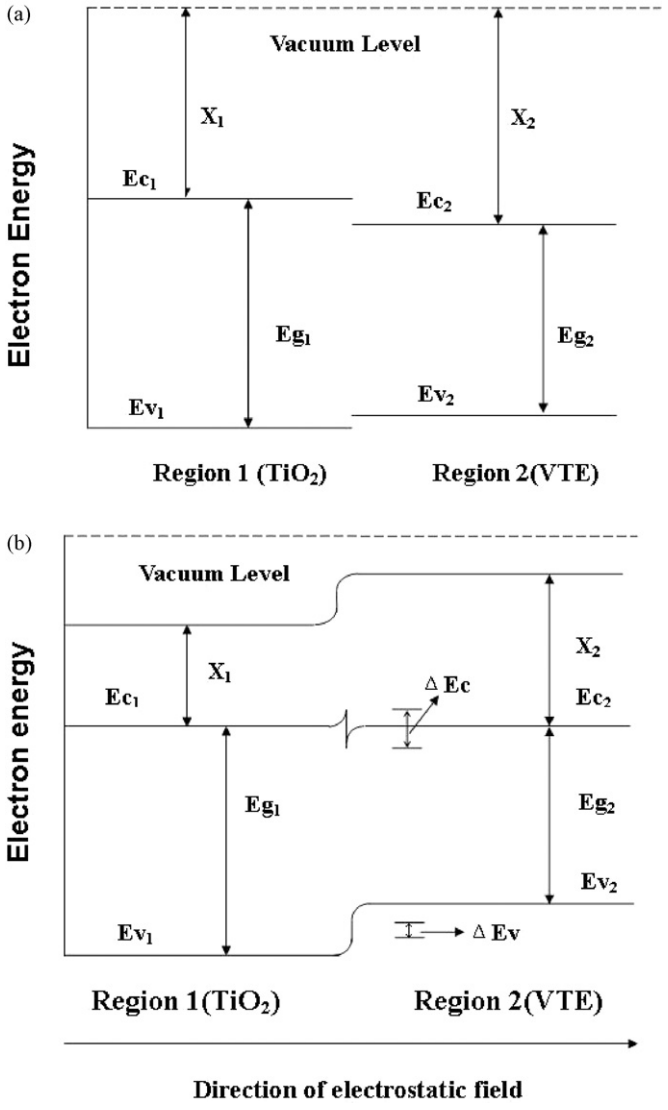

Fig. 10. Equilibrium energy band diagrams of TiO_2/V–TiO_2 composite photocatalysts before (a) and after (b) the formation of n–n heterojunction.

mixture as listed in Table 1 was the same as that of the pure TiO_2, indicating that the intimate contact between undoped TiO_2 with 0.5%V–TiO_2 is crucial for the formation of n–n heterojunction.

4.2. Effect of ammonium oleate

The isoelectric point (IEP) was reported to be at pH 5.8, 6.0, 6.4, 6.0 and 5.8 for pure titania, 0.5%V–TiO_2, 1%V–TiO_2, 1.4%V–TiO_2 and 2.5%V–TiO_2, respectively [98]. The surface of transparent colloidal titania nanoparticles and VTE was positively charged at the pHs in the TiO_2-sol (pH 4). The surface of z%V–TiO_2-O nanoparticles was negatively charged because the oleate anions had been adsorbed onto the surface of VTE nanoparticles. In the case of VTMU nanoparticles, when z%V–TiO_2-O nanoparticles were added into TiO_2-sol, transparent colloidal titania nanoparticles (positively charged) would link up with z%V–TiO_2-O nanoparticles (negatively charged) because of electrostatic attraction. After the drying and calcination, amorphous colloidal titania nanoparticles changed into crystalline anatase nanoparticles and ammonium oleate was thermally decomposed [106–110], then at the interface between anatase nanoparticles with VTE nanoparticles, the n–n heterojunction would be formed because of the sintering

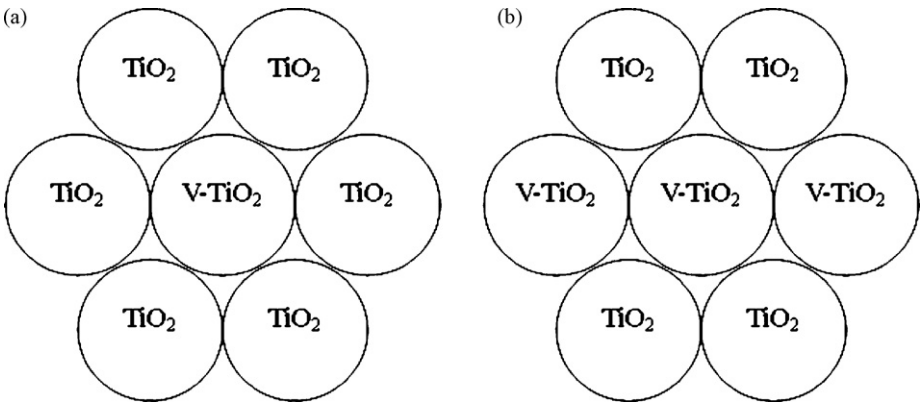

Fig. 11. Schematic diagrams in two dimensions of the configuration of TiO_2/V–TiO_2 composite photocatalysts if (a) V–TiO_2 particles are not agglomerated, and (b) V–TiO_2 particles are agglomerated.

between anatase nanoparticles with VTE nanoparticles. But in the case of VTU nanoparticles, when *z*%V–TiO_2-O nanoparticles were added into TiO_2-sol, electrostatic repulsion between positively charged colloidal titania nanoparticles with positively charged *z*%V–TiO_2 nanoparticles might obstruct the adhesion of colloidal titania nanoparticles on *z*%V–TiO_2 nanoparticles. So, *z*%V–TiO_2-O nanoparticles combine with undoped titania more tightly than *z*%V–TiO_2 nanoparticles. Therefore, the interface region (n–n heterojunction region) in VTMU can be expected to be larger than that in VTU, as a result, the photocatalytic activity of the former was higher than that of the latter (comparing *y*TiO_2/0.5%V–TiO_2/M with *y*TiO_2/0.5%V–TiO_2). In addition, the higher photocatalytic activity of VTMU should be partly due to the slightly higher specific surface area (e.g. comparing 12TiO_2/0.5%V–TiO_2/M with 12TiO_2/0.5%V–TiO_2).

4.3. Effect of y

Since the content of vanadium in composite photocatalysts is very low, there is no suitable technique to be used to analyze the microstructure of composite photocatalysts. So, in this paper, a hypothetical configuration of composite photocatalysts is proposed. We assume that for TiO_2/V–TiO_2 composite photocatalysts, V–TiO_2 and undoped TiO_2 particles are all equal-diameter spherical particles, and every V–TiO_2 particle is not contacted with other V–TiO_2 particles (i.e. V–TiO_2 particles are not agglomerated). The configuration of TiO_2/V–TiO_2 composite photocatalysts is similar to that of the metals with close-packed structures [111]. The schematic diagrams in two dimensions are illustrated in Fig. 11. Each V–TiO_2 particle is contacted with 12 undoped TiO_2 particles (Fig. 11a), which leads to the formation of 12 regions of n–n heterojunction.

Let us consider the number (N_{nn}) of regions of n–n heterojunction in 1 mol TiO_2/V–TiO_2 composite photocatalysts. For $y = 12$ (y is the nominal molar ratio of titania of undoped TiO_2 to that of VTE), each V–TiO_2 particle is exactly contacted with 12 undoped TiO_2 particles,

$$N_{nn} = \frac{12w}{(12+1)\,\rho V}; \tag{1}$$

for $y > 12$, each V–TiO_2 particle is contacted with 12 undoped TiO_2 particles and the remaining undoped TiO_2 particles cannot lead to the formation of regions of n–n heterojunction,

$$N_{nn} = \frac{12w}{(y+1)\,\rho V}; \tag{2}$$

for $y < 12$, each V–TiO_2 particle is contacted with y undoped TiO_2 particles,

$$N_{nn} = \frac{yw}{(y+1)\,\rho V}, \tag{3}$$

where w is molar weight of titania (79.88 g/mol), ρ is the density of anatase (3.83 g/cm^3), and V is the volume of each titania particle. For simplicity, we assume the particle size of each titania particle is 20 nm, then V equals 4.187×10^{-18} cm^3. The calculated values of N_{nn} are listed in Table 1.

If V–TiO_2 particles are agglomerated, the number of undoped TiO_2 particles contacting with one V–TiO_2 particle is less than 12, which results in the decrease in the number of regions of n–n heterojunction and consequently reduces photoactivity. For example, if one V–TiO_2 particle has already connected with two V–TiO_2 particles, only 10 undoped TiO_2 particles can be contacted with this V–TiO_2 particle (Fig. 11b).

From Table 1, it is clear that N_{nn} increases with an increase of y up to 12 followed by a decrease with further increase of y. So we infer that 12TiO_2/*z*%V–TiO_2/M and 12TiO_2/*z*%V–TiO_2 will achieve the best performance compared with other *y*TiO_2/*z*%V–TiO_2/M (y is not 12) and *y*TiO_2/*z*%V–TiO_2 (y is not 12), respectively. That is to say, for TiO_2/V–TiO_2 composite photocatalysts, the optimal nominal molar ratio of titania of undoped TiO_2 to that of VTE equals 12. If V–TiO_2 particles are agglomerated, the optimal nominal molar ratio will decrease. As shown in Table 1 and Fig. 2, for photocatalysts *y*TiO_2/0.04%V–TiO_2/M, *y*TiO_2/0.5%V–TiO_2/M, *y*TiO_2/2%V–TiO_2/M and *y*TiO_2/0.5%V–TiO_2, the optimal values of y are 11, 12, 8 and 12, respectively. These data imply that the above-mentioned analyses are reasonable.

4.4. Effect of vanadium dopant concentration

The built-in electric field strength of space-charge region in n–n heterojunction increases with the increase of the absolute value of difference of Fermi energy between the materials on the two sides [103,104]. As mentioned above, Anderson et al. [98] have found that the Fermi energy of V-doped titania decreases with the increase of vanadium dopant concentration. So, with increasing vanadium dopant concentration, the built-in electric field strength increase and therefore the photo-generated electron–hole pairs separate more quickly under illumination.

On the other hand, the spike formed in the conduction band at the interface (Fig. 10) may prevent flow of the photo-generated electrons [112]. The higher the vanadium dopant concentration is, the larger the conduction band edge discontinuity is (since $\Delta E_c = x_2 - x_1 \approx E_{F1} - E_{F2}$). Therefore, for samples with higher vanadium dopant concentration, the conduction-band spike barrier is

relatively larger, which is detrimental to the photocatalytic activity. Additionally, for samples with higher vanadium dopant concentration, dopants act more as recombination centers than as trap sites for charge transfer, which leads to the reduced activity in spite of they can absorb more of the photons, which is beneficial to the photoactivity. So an optimal vanadium dopant concentration (0.5% in this study) in TiO_2/V–TiO_2 composite photocatalysts exists for maximum photocatalytic efficiency. Moreover, for TiO_2/V–TiO_2 composite photocatalysts, vanadium ions in the VTE side can probably diffuse into undoped titania particles side after calcination; the higher the concentration of vanadium in VTE and the more the amounts of VTE added into TiO_2-sol, the more the extent of diffusion of vanadium ions. As a result, for TiO_2/V–TiO_2 composite photocatalysts with higher dopant concentration and with low value of y (for example, 4TiO_2/2%V–TiO_2/M), the excess dopants in undoped titania particles side act as recombination centers, which is detrimental to the photoactivity.

As shown in Fig. 1 and Table 1, P25 Degussa commercial powder is the best photocatalyst compared with the photocatalysts prepared in this study. It must be noted that P25 is a mixture of rutile and anatase. Rutile itself is a low-active phase, but the junction created by the two semiconductors helps the charge-carriers separation. The rutile phase of P25 plays the role of charges separation and provides sites for oxidation [113,114]. In that case, P25 is difficult to compare to the anatase phases.

5. Conclusions

Highly active TiO_2/V–TiO_2 composite photocatalysts were synthesized by a modified method using ammonium oleate in order to improve the structure of n–n heterojunction, i.e. by mixing TiO_2 sol with sol–gel derived V–TiO_2 powders that have adsorbed ammonium oleate in advance, followed by drying and calcination. TiO_2/V–TiO_2 composite photocatalysts were generally shown to have a much higher photocatalytic destruction rate than that of undoped TiO_2, which is ascribed mainly to the electrostatic-field-driven electron–hole separation in TiO_2/V–TiO_2 composite photocatalysts. An optimal vanadium dopant concentration (0.5% in this study) and an optimal y (the nominal molar ratio of titania of undoped TiO_2 to VTE) in TiO_2/V–TiO_2 composite photocatalysts exist for maximum photocatalytic efficiency. A hypothesis was proposed to explain the existence of these optimal values.

Acknowledgement

This work was supported under Open Funds awarded by the Key Lab of Enhanced Heat Transfer and Energy Conservation, Ministry of Education, China.

References

[1] W. Choi, A. Termin, M.R. Hoffmann, J. Phys. Chem. 98 (1994) 13669.
[2] K. Nagaveni, M.S. Hegde, G. Madras, J. Phys. Chem. B 108 (2004) 20204.
[3] M. Gratzel, R.F. Howe, J. Phys. Chem. 94 (1990) 2566.
[4] S.T. Martin, C.L. Morrison, M.R. Hoffmann, J. Phys. Chem. 98 (1994) 13695.
[5] K. Bhattacharyya, S. Varma, A.K. Tripathi, S.R. Bharadwaj, A.K. Tyagi, J. Phys. Chem. C 112 (2008) 19102.
[6] N. Serpone, D. Lawless, J. Disdier, J.M. Herrmann, Langmuir 10 (1994) 643.
[7] A. Fuerte, M.D. Hernandez-Alonso, A. Maira, A. Martinez-Arias, M. Fernandez-Garcia, J.C. Conesa, J. Soria, Chem. Commun. (2001) 2718.
[8] S. Ikeda, N. Sugiyama, B. Pal, G. Marci, L. Palmisano, H. Noguchi, K. Uosaki, B. Ohtani, Phys. Chem. Chem. Phys. 3 (2001) 267.
[9] A. Di Paola, G. Marci, L. Palmisano, M. Schiavello, K. Uosaki, B. Ohtani, J. Phys. Chem. B 106 (2002) 637.
[10] A. Di Paola, E. Garcia-Lopez, S. Ikeda, G. Marci, B. Ohtani, L. Palmisano, Catal. Today 75 (2002) 87.
[11] S.M. Karvinen, Ind. Eng. Chem. Res. 42 (2003) 1035.
[12] Z. Luo, Q.H. Gao, J. Photochem. Photobiol. A: Chem. 63 (1992) 367.
[13] A. Fuerte, M.D. Hernandez-Alonso, A.J. Martinez-Arias, M. Fernández-Gareía, J.C. Conesa, J. Soria, Chem. Commun. (2001) 2718.
[14] S. Klosek, D. Raftery, J. Phys. Chem. B 105 (2001) 2815.
[15] K. Iketani, R.D. Sun, M. Toki, K. Hirota, O. Yamaguchi, Mater. Sci. Eng. B 108 (2004) 187.
[16] J.C.S. Wu, C.H. Chen, J. Photochem. Photobiol. A: Chem. 163 (2004) 509.
[17] M.M. Mohamed, M.M. Al-Esaimi, J. Mol. Catal. A: Chem. 255 (2006) 53.
[18] J.K. Zhou, M. Takeuchi, A.K. Ray, M. Anpo, X.S. Zhao, J. Colloid Interface Sci. 311 (2007) 497.
[19] M. Bettinelli, V. Dallacasa, D. Falcomer, P. Fornasiero, V. Gombac, T. Montini, L. Romano, A. Speghini, J. Hazard. Mater. 146 (2007) 529.
[20] X. Yang, C. Cao, K. Hohn, L. Erickson, R. Maghirang, D. Hamal, K. Klabunde, J. Catal. 252 (2007) 296.
[21] D. Masih, H. Yoshitake, Y. Izumi, Appl. Catal. A: Gen. 325 (2007) 276.
[22] F. Bertinchamps, M. Treinen, P. Eloy, A.-M. DosSantos, M.M. Mestdagh, E.M. Gaigneaux, Appl. Catal. B: Environ. 70 (2007) 360.
[23] J.C. Yu, J. Lin, R.W.M. Kwok, J. Photochem. Photobiol. A: Chem. 111 (1997) 199.
[24] N. Namiki, K. Cho, P. Fraundorf, P. Biswas, Ind. Eng. Chem. Res. 44 (2005) 5213.
[25] W.J. Hong, S. Kang, Mater. Lett. 60 (2006) 1296.
[26] K. Bhattacharyya, S. Varma, A.K. Tripathi, S.R. Bharadwaj, A.K. Tyagi, J. Phys. Chem. B 113 (2009) 5917.
[27] Z. Zhao, Q. Liu, Catal. Lett. 124 (2008) 111.
[28] H. Li, G. Zhao, G. Han, B. Song, Surf. Coat. Technol. 201 (2007) 7615.
[29] D. Gu, B. Yang, Y. Hu, Catal. Lett. 118 (2007) 254.
[30] S. Neatu, E. Sacaliuc-Parvulescu, F. Levy, V.I. Parvulescu, Catal. Today 142 (2009) 165.
[31] L. Li, C. Liu, Y. Liu, Mater. Chem. Phys. 113 (2009) 551.
[32] M.A. Rauf, S.B. Bukallah, A. Hamadi, A. Sulaiman, F. Hammadi, Chem. Eng. J. 129 (2007) 167.
[33] B. Liu, X. Wang, G. Cai, L. Wen, Y. Song, X. Zhao, J. Hazard. Mater. 169 (2009) 1112.
[34] A.J. Nozik, Appl. Phys. Lett. 30 (1977) 567.
[35] N. Serpone, P. Maruthamuthu, P. Pichat, E. Pelizzetti, H. Hidaka, J. Photochem. Photobiol. A: Chem. 85 (1995) 247.
[36] A.H. Zyoud, N. Zaatar, I. Saadeddin, C. Ali, D. Park, G. Campet, H.S. Hilal, J. Hazard. Mater. 173 (2010) 318.
[37] J.S. Jang, S.M. Ji, S.W. Bae, H.C. Son, J.S. Lee, J. Photochem. Photobiol. A: Chem. 188 (2007) 112.
[38] J.C. Yu, L. Wu, J. Lin, P. Li, Q. Li, Chem. Commun. (2003) 1552.
[39] P.A. Sant, P.V. Kamat, Phys. Chem. Chem. Phys. 4 (2004) 198.
[40] S. Biswas, M.F. Hossain, T. Takahashi, Y. Kubota, A. Fujishima, Phys. Stat. Sol. A 205 (2008) 2028.
[41] J.C. Tristão, F. Magalhães, P. Corio, M.T.C. Sansiviero, J. Photochem. Photobiol. A: Chem. 181 (2006) 152.
[42] J.S. Jang, H.G. Kim, U.A. Joshi, J.W. Jang, J.S. Lee, Int. J. Hydrogen Energy 33 (2008) 5975.
[43] H. Fujii, M. Ohtaki, K. Eguchi, H. Arai, J. Mol. Catal. A: Chem. 129 (1998) 61.
[44] M. Takahashi, H. Natori, K. Tajima, K. Kobayashi, Thin Solid Films 489 (2005) 205.
[45] Y. Bessekhouad, D. Robert, J.V. Weber, J. Photochem. Photobiol. A: Chem. 163 (2004) 569.
[46] C.Y. Yang, W.D. Wang, Z.C. Shan, F.Q. Huang, J. Solid State Chem. 182 (2009) 807.
[47] W. Ho, J.C. Yu, J. Lin, J.G. Yu, P. Li, Langmuir 20 (2004) 5865.
[48] R. Brahimi, Y. Bessekhouad, A. Bouguelia, M. Trari, J. Photochem. Photobiol. A: Chem. 194 (2008) 173.
[49] S.C. Lo, C.F. Lin, C.H. Wu, P.H. Hsieh, J. Hazard. Mater. 114 (2004) 183.
[50] S. Chen, W. Zhao, W. Liu, S. Zhang, Appl. Surf. Sci. 255 (2008) 2478.
[51] J. Tian, L. Chen, Y. Yin, X. Wang, J. Dai, Z. Zhu, X. Liu, P. Wu, Surf. Coat. Technol. 204 (2009) 205.
[52] Y.Z. Lei, G.H. Zhao, M.C. Liu, Z.N. Zhang, X.L. Tong, T.C. Cao, J. Phys. Chem. C 113 (2009) 19067.
[53] D. Chen, H. Zhang, S. Hu, J.H. Li, J. Phys. Chem. C 112 (2008) 117.
[54] S. Chen, S. Zhang, W. Liu, W. Zhao, J. Hazard. Mater. 155 (2008) 320.
[55] Y.G. Zhang, L.L. Ma, J.L. Li, Y. Yu, Environ. Sci. Technol. 41 (2007) 6264.
[56] Y. Bessekhouad, D. Robert, J.V. Weber, Catal. Today 101 (2005) 315.
[57] F.R. Xiu, F.S. Zhang, J. Hazard. Mater. 172 (2009) 1458.
[58] I. Bejia, P.V. Kamat, J. Phys. Chem. 99 (1995) 9182.
[59] S. Chen, L. Chen, S. Gao, G. Cao, Mater. Chem. Phys. 98 (2006) 116.
[60] L.Y. Shi, C.Z. Li, H.C. Gu, D.Y. Fang, Mater. Chem. Phys. 62 (2000) 62.
[61] K. Vinodgopal, I. Bedja, P.V. Kamat, Chem. Mater. 8 (1996) 2180.
[62] J. Shang, W.Q. Yao, Y.F. Zhu, N.Z. Wu, Appl. Catal. A: Gen. 257 (2004) 25.
[63] T. Kawahara, Y. Konishi, H. Tada, N. Tohge, S. Ito, Langmuir 17 (2001) 7442.
[64] H. Tada, A. Hattori, Y. Tokihisa, K. Imai, N. Tohge, S. Ito, J. Phys. Chem. B 104 (2000) 4585.
[65] T. Ohno, F. Tanigawa, K. Fujihara, S. Izumi, M. Matsumura, J. Photochem. Photobiol. A: Chem. 118 (1998) 41.
[66] S. Chen, L. Chen, S. Gao, G. Cao, Powder Technol. 160 (2005) 198.
[67] E.V. Skorb, E.A. Ustinovich, A.I. Kulak, D.V. Sviridov, J. Photochem. Photobiol. A: Chem. 193 (2008) 97.
[68] F. Ye, A. Ohmori, C. Li, Surf. Coat. Technol. 184 (2004) 233.
[69] F. Ye, A. Ohmori, C. Li, J. Mater. Sci. 39 (2004) 353.
[70] B. Gao, Y.J. Kim, A.K. Chakraborty, W.I. Lee, Appl. Catal. B: Environ. 83 (2008) 202.
[71] H.J. Huang, D.Z. Li, Q. Lin, W.J. Zhang, Y. Shao, Y.B. Chen, M. Sun, X.Z. Fu, Environ. Sci. Technol. 43 (2009) 4164.
[72] G.C. Xiao, X.C. Wang, D.Z. Li, X.Z. Fu, J. Photochem. Photobiol. A: Chem. 193 (2008) 213.

[73] R. Brahimi, Y. Bessekhouad, A. Bouguelia, M. Trari, J. Photochem. Photobiol. A: Chem. 186 (2007) 242.
[74] J. Qu, X. Zhao, Environ. Sci. Technol. 42 (2008) 4934.
[75] H. Yu, S. Chen, X. Quan, H. Zhao, Y. Zhang, Environ. Sci. Technol. 42 (2008) 3791.
[76] T. Omata, S. Otsuka-Yao-Matsuo, J. Photochem. Photobiol. A: Chem. 156 (2003) 243.
[77] C.Y. Lin, Y.K. Fang, C.H. Kuo, S.F. Chen, C.S. Lin, T.H. Chou, Y.H. Lee, J.C. Lin, S.B. Hwang, Appl. Surf. Sci. 253 (2006) 898.
[78] I.C. Kang, Q. Zhang, S. Yin, T. Sato, F. Saito, Sci. Technol. 42 (2008) 3622.
[79] M. Niu, F. Huang, L. Cui, P. Huang, Y. Yu, Y. Wang, ACS Nano 4 (2010) 681.
[80] L. Cui, F. Huang, M. Niu, L. Zeng, J. Xu, Y. Wang, J. Mol. Catal. A: Chem. 326 (2010) 53.
[81] S. Liu, T.H. Xie, Z. Chen, J.T. Wu, Appl. Surf. Sci. 255 (2009) 8587.
[82] C.B. Rodella, P.A.P. Nascente, R.W.A. Franco, C.J. Magon, V.R. Mastelaro, A.O. Florentino, Phys. Stat. Sol. A 187 (2001) 161.
[83] S.J. Gregg, K.S. Sing, Adsorption, Surface Area and Porosity, 2nd ed., Academic Press, London, 1982.
[84] M.H. Zhou, J.G. Yu, B. Cheng, H.G. Yu, Mater. Chem. Phys. 93 (2005) 159.
[85] Z. Zhang, V.E. Henrich, Surf. Sci. 277 (1992) 263.
[86] M. Sambi, G. Sangiovanni, G. Granozzi, Phys. Rev. B 55 (1997) 7850.
[87] Q. Sun, Y. Fu, J. Liu, A. Auroux, J. Shen, Appl. Catal. A: Gen. 334 (2008) 26.
[88] M.A. Bañares, L.J. Alemany, M.C. Jiménez, M.A. Larrubia, F. Delgado, M.L. Granados, A. Martínez-Arias, J.M. Blasco, J.L.G. Fierro, J. Solid State Chem. 124 (1996) 69.
[89] X. Lü, J. Li, X. Mou, J. Wu, S. Ding, F. Huang, Y. Wang, F. Xu, J. Alloys Compd. 499 (2010) 160.
[90] N.D. Abazovic, M.I. Comor, M.D. Dramicanin, D.J. Jovanovic, S.P. Ahrenkiel, J.M. Nedeljkovic, J. Phys. Chem. B 110 (2006) 25366.
[91] M.M. Rahman, K.M. Krishna, T. Soga, T. Jimbo, M. Umeno, J. Phys. Chem. Solids 60 (1999) 201.
[92] H. Tang, H. Berger, P.E. Schmid, F. Levy, Solid State Commun. 87 (1993) 847.
[93] J.K. Zhou, Y.X. Zhang, X.S. Zhao, A.K. Ray, Ind. Eng. Chem. Res. 45 (2006) 3503.
[94] C.K. Liau, W. Chou, Microelectron. Eng. 86 (2009) 361.
[95] J.M. Herrmann, J. Disdier, G. Deo, I.E. Wachs, J. Chem. Soc. Faraday Trans. 93 (1997) 1655.
[96] D. Morris, R.G. Egdell, J. Mater. Chem. 11 (2001) 3207.
[97] G. Zhao, G. Han, Int. J. Mod. Phys. B 16 (2002) 4465.
[98] J.J. Sene, W.A. Zeltner, M.A. Anderson, J. Phys. Chem. B 107 (2003) 1597.
[99] Y.Q. Wang, Y.Z. Hao, H.M. Cheng, J.M. Ma, B. Xu, W.H. Li, S.M. Cai, J. Mater. Sci. 34 (1999) 2773.
[100] M. Grätzel, F.P. Rotzinger, Chem. Phys. Lett. 118 (1985) 474.
[101] R.A. Smith, Semiconductors, 2nd ed., Cambridge University Press, London, 1978.
[102] B.L. Sharma, R.K. Purohit, Semiconductor Heterojunctions, Pergamon Press, Oxford, 1974.
[103] R.C. Kumar, Solid State Electron. 11 (1968) 543.
[104] S.I. Cserveny, Int. J. Electron. 25 (1968) 65.
[105] D. Duonghong, J. Ramsden, M. Grätzel, J. Am. Chem. Soc. 104 (1982) 2977.
[106] P. Falciola, Gazz. Chim. Ital. 40 (1911) 217.
[107] G. Bornemann, Chem.-Zeitung 32 (1908) 741.
[108] F.I. Khattab, N.A. Al-Ragehy, A.K.S. Ahmad, Thermochim. Acta 73 (1984) 47.
[109] G. Gnanaprakash, S. Ayyappan, J. Philip, B. Raj, Nanotechnology 17 (2006) 5851.
[110] P. Roonasi, A. Holmgren, Appl. Surf. Sci. 255 (2009) 5891.
[111] R.C. Evans, An Introduction to Crystal Chemistry, 2nd ed., Cambridge University Press, London, 1964.
[112] M. Ichimura, Sol. Energy Mater. Sol. Cells 93 (2009) 375.
[113] R.I. Bickley, T. Gonzalez-Carreno, J.S. Lees, L. Palmisano, R.J.D. Tilley, J. Solid State Chem. 92 (1991) 178–190.
[114] Yu.V. Kolen'ko, A.V. Garshev, B.R. Churagulov, S. Boujday, P. Portes, C. Colbeau-Justin, J. Photochem. Photobiol. A: Chem. 172 (2005) 19–26.